Superconducting Properties of *(MnFe$_2$O$_4$)$_x$/CuTl-1223* Composites

Rashid Khan, M. Mumtaz*

Materials Research Laboratory, Department of Physics, Faculty of Basic and Applied Sciences (FBAS), International Islamic University (IIU) Islamabad 44000, Pakistan

*Corresponding author: M. Mumtaz, Materials Research Laboratory, Department of Physics, Faculty of Basic and Applied Sciences (FBAS), International Islamic University (IIU) Islamabad 44000, Pakistan. Tel: +92-51-9019926 (Office), Fax No: +92-51-9210256; E-mail: mmumtaz75@yahoo.com

Abstract

The effects of nanometer size MnFe$_2$O$_4$ particles addition on different properties of (Cu$_{0.5}$Tl$_{0.5}$) Ba$_2$Ca$_2$Cu$_3$O$_{10-\delta}$ (CuTl-1223) superconducting phase was studied. MnFe$_2$O$_4$ nanoparticles were synthesized by sol-gel method and were added to CuTl-1223 superconducting phase synthesized by solid-state reaction to get *(MnFe$_2$O$_4$)$_x$/CuTl-1223*; x = 0 ~ 2.0 wt. % composites. The effects of these magnetic nanoparticles on structural, morphological and superconducting transport properties of host CuTl-1223 phase were investigated via X-ray diffraction (XRD), scanning electron microscopy (SEM), energy dispersive X-rays (EDX) spectroscopy, Fourier transform infrared (FTIR) spectroscopy and Four-Probe Resistivity (ρ) measurements. Inclusion of these nanoparticles exhibited no change in crystal structure of host CuTl-1223 superconducting phase. Suppression of superconducting properties was probably due to enhanced effective scattering of carriers across magnetic natured MnFe$_2$O$_4$ nanoparticles residing at the grain-boundaries of CuTl-1223 superconductor.

Introduction

Selection of any superconducting material for practical applications highly depends upon different critical parameters like critical temperature (T$_c$), critical current density (J$_c$) and critical magnetic field (H$_c$). Different phases of Cu$_{0.5}$Tl$_{0.5}$Ba$_2$Ca$_{n-1}$Cu$_n$O$_{2n+4-\delta}$ high temperature superconductor (HTSCs) family can be synthesized at higher pressure of (~5 GPa) as well as at ambient pressure[1]. HTSCs samples synthesized at high pressure exhibited relatively higher superconducting properties due to reduction in bulk porosity and higher value of superconducting volume fraction. But large scale production of HTSCs at higher pressure for industrial based applications is a biggest challenge in present time. Therefore, synthesis of HTSCs at ambient pressure is an appropriate way for large production. But presence of voids and pores in higher density is the main

disadvantage of this synthesis route, which reduces overall superconducting volume fraction. Another reason for reduction in carrier's density from an optimal level is mostly caused by the existence of various defects in the form of oxygen deficiencies in ambient pressure synthesized HTSCs samples. So, other than higher pressure synthesis route, numbers of efforts have been made to overcome this problem in which main goal was to improve the superconducting properties of different compounds of HTSCs families by different techniques[2-4]. This issue is most effectively resolved by increasing the connectivity between the grains and reduction in density of voids and pores by inclusion of various nanoparticles, which is the easiest and efficient ways in this regards. But control on the size, concentration and distribution of these nanoparticles at grain-boundaries of host bulk HTSCs are the real challenges[5-8]. This uniform distribution of nanoparticles can equally facilitate the transportation of

charge carriers across the grain-boundaries but up to a certain optimal level of nanoparticles inclusion after which prominent reduction in superconducting volume fraction takes place. It was found that nature of nanostructures materials added in the host material plays a very crucial role in deciding the resultant effects on superconducting properties. A prominent improvement in superconducting properties of Bi-based superconductor was observed after inclusion of MgO, ZrO_2 and Al_2O_3 nanoparticles[9-11]. Increase in superconducting volume fraction and sharpness in transition width of Bi-2212 superconducting phase was observed after inclusion of MgO nanoparticles[12]. The critical current density, volume pinning force density, activation energy and onset temperature in presence of applied magnetic field were improved after alumina nanoparticles inclusion in (Bi, Pb)-2223 superconductor[13]. The inclusion of various nanoparticles of different materials with variant sizes like Fe_2O_3 with required amount was used to generate the artificial flux pinning centers, which can increase the various infield superconducting parameters[14]. The crystal structure and J_c value of Y123 superconducting thin film improved after the addition of Ag nanoparticles[15]. Addition of Ag nanoparticles improved the superconducting and mechanical properties of Bi(Pb)-Sr-Ca-Cu-O superconducting phase, which was attributed to the cementing effects of these metallic nanoparticles at grain-boundaries[16]. An improvement was observed in critical parameters and superconducting volume fraction of CuTl-1223 matrix after addition of Ag nanoparticles up to x = 1.5 wt. %[17]. Addition of $ZnFe_2O_4$ nanoparticles in Gd-$Ba_2Cu_3O_{7-\delta}$ enhanced superconducting parameters up to a certain optimal concentration level[18]. $CoFe_2O_4$ nanoparticles addition in $YBa_2Cu_3O_7$ (Y-123) and $Y_3Ba_5Cu_8O_{18}$ (Y-358) highly suppressed the superconducting parameters as well as grain size[19]. The critical current density J_c of Bi-2223 superconductor was increased after inclusion $NiFe_2O_4$ nanoparticles[20].

In this article, we have analyzed and compared the effects of ferri-magnetic $MnFe_2O_4$ nanoparticles inclusion on structural, morphological and electric transport properties of CuTl-1223 phase in detail. In literature there is no evidence of investigation on the effects of these nanoparticles inclusion in HTSCs materials.

Experimental details

Solid-state reaction method was used to prepare bulk $Cu_{0.5}Ba_2Ca_2Cu_3O_{10-\delta}$ precursor. Initially $Cu_2(CN).H_2O$ (99%, BDH), $Ba(NO_3)_2$ (99.50%, UNI-Chem), and $Ca(NO_3)_2 \cdot 4H_2O$ (99%, Sigma-Aldrich) were mixed in suitable ratios of 5.149, 7.802 and 7.049 grams to prepared 20 grams initial mixture, which was ground for 4 hours in agate motor and pestle to get fine powder. Then fine ground powder was placed in a quartz boat and was heat-treated at 860ºC for 24 hours in pre-heated chamber furnace. The heat-treatment process was repeated with intermediate grinding of 1 hour and each time furnace was cooled down to room temperature to finally obtain $Cu_{0.5}Ba_2Ca_2Cu_3O_{10-\delta}$ precursor.

$MnFe_2O_4$ nanoparticles were separately prepared by conventional sol-gel method. Initially we prepared two solutions, one which contain 2.5 gm of manganese nitrate $Mn(NO_3)_2$ (99.99%, Sigma-Aldrich) and 8 gm of iron nitrate (99.95%, Sigma-Aldrich) mixture in 10 ml ethanol (99.8%, Sigma-Aldrich). Another solution containing mixture of 15 ml of distilled water and 5.7 gm of citric acid (99.5%, Sigma-Aldrich) was prepared

separately. Now slowly mixed both solutions with continuous stirring and then adjusted its pH to 5 by adding ammonia solution drop by drop into the final solution. Now heat is maintained at 75ºC during continuous stirring. This process continued until solution was converted into gel. The gel was dried in an oven at 110ºC for overnight. The dried gel was then annealed at 900ºC in order to get $MnFe_2O_4$ nanoparticles.

Various concentrations of $MnFe_2O_4$ nanoparticles and Tl_2O_3 (99%, BDH) were added to $Cu_{0.5}Ba_2Ca_2Cu_3O_{10-\delta}$ precursor in specific required concentrations. These mixed materials were ground for 1 hour and then pellets were made by using of hydraulic press. Each pellet was enclosed in a gold capsule and sintered in pre-heated chamber furnace at 860ºC for 10 min and quenched to room temperature to get required *(MnFe₂O₄)ₓ/CuTl-1223* nanoparticles-superconductor composites.

Results and Discussion

Crystal structures of nanoparticles and superconducting composites were determined by XRD technique. XRD pattern of $MnFe_2O_4$ nanoparticles is shown in Figure.1. Debye-Scherrer's formula was used to determine the average particle size and was found 20 nm. All the major well indexed diffraction peaks demonstrate the spinal structure of $MnFe_2O_4$ nanoparticles. $MnFe_2O_4$ showed cubic structure following space group Fd-3m with calculated lattice parameter a = 4.89Å. XRD spectra of *(MnFe₂O₄)ₓ/CuTl-1223* composites are shown in Figure.2. Majority of XRD peaks of these composites are indexed according tetragonal structure of CuTl-1223 phase following P4/mmm space group[21]. XRD of all these samples have also shown the presence of very small amount of impurities and other superconducting phases. Percentage volume fraction of different phases was calculated by using the following relations:

$$CuTl\text{-}(1223)\ \% = \frac{\sum I(1223)}{\sum\{I(1223)+I(1234)I+(1212)+I(Unknown\ Impurities)\}} \times 100$$

$$CuTl\text{-}(1234)\ \% = \frac{\sum I(1234)}{\sum\{I(1223)+I(1234)+I(1212)+I(Unknown\ Impurities)\}} \times 100$$

$$CuTl\text{-}(1212)\ \% = \frac{\sum I(1212)}{\sum\{I(1223)+I(1234)+I(1212)+I(Unknown\ Impurities)\}} \times 100$$

$$Unknown\ Impurities\ \% = \frac{\sum I(Unknown\ Impurities)}{\sum\{I(1223)+I(1234)+I(1212)+I(Unknown\ Impurities)\}} \times 100$$

Where, I (1223), I (1234), I (1212) and I (Impurities) are intensities of respective XRD peaks for CuTl-1223, CuTl-1234, CuTl-1212 phases and unknown impurities, respectively. The calculated relative proportions of these phases present in *(MnFe₂O₄)ₓ/CuTl-1223* composites are listed in Table 1. We observed a clear decrease in % of volume fraction of CuTl-1223 phase with the addition of $MnFe_2O_4$ nanoparticles. The intensities of diffraction peaks related to nanoparticles crystal structures are very small, which are suppressed under high intensities diffraction peaks of host CuTl-1223 superconductor. But all the major diffraction peaks are well indexed according to CuTl-1223 phase after addition of $MnFe_2O_4$ nanoparticles, which indicates unaltered crystal structure of host CuTl-1223 matrix.
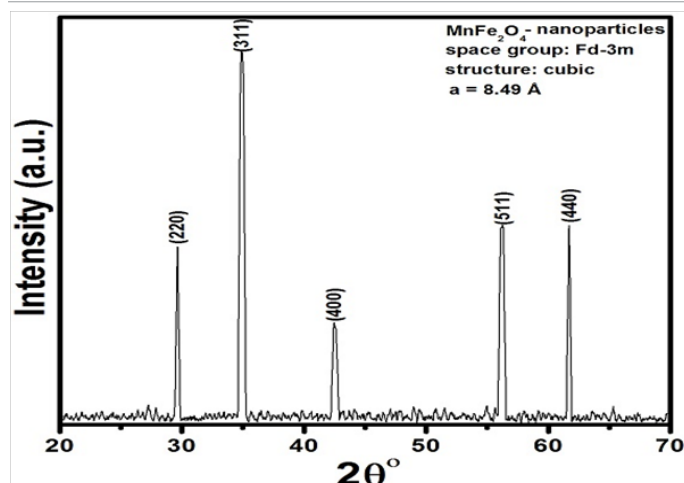
Figure 1. XRD spectrum of (MnFe₂O₄) nanoparticles.

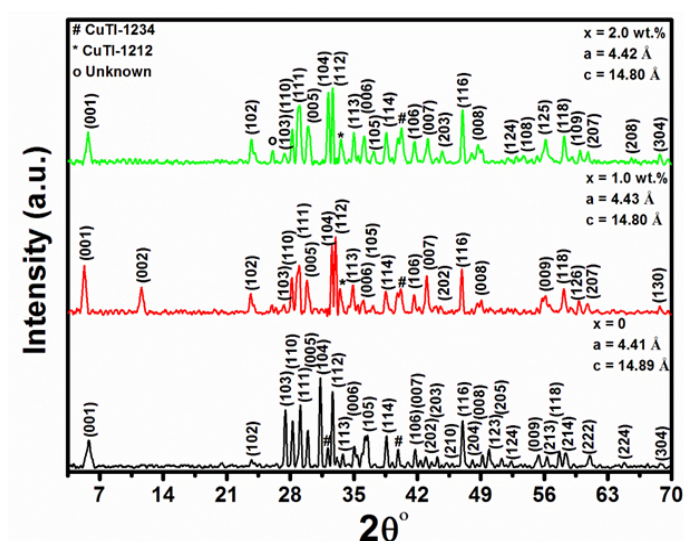**Figure 2**. XRD spectra of $(MnFe_2O_4)_x/(CuTl\text{-}1223)$; x = 0, 1.0 and 2.0 wt.% composites.

Table 1. % volume fraction of CuTl-1223, CuTl-1234, CuTl-1212 and unknown impurities present in $(MnFe_2O_4)_x/CuTl\text{-}1223$ nanoparticles-superconductor composites x = 0, 1.0 and 2.0 wt. %.

% volume fraction of different phases and unknown impurities				
Nanoparticles contents (x %)	% of CuTl-1223 Phase	% of CuTl-1234 Phase	% of CuTl-1212 Phase	% of Unknown Impurities
0	94.49	4.9	0.55	----
1.0	91.48	3.54	3.59	1.31
2.0	90.50	4.54	3.15	1.78

Morphology of representative $(MnFe_2O_4)_x/CuTl\text{-}1223$; x = 0 and 1.0 wt.% composites samples was examined by scanning electron microscope(SEM) as shown in Figure.3. We observed relative improvement in inter-grain weak-links and decrease in density of voids and pores after addition MnFe₂O₄ nanoparticles in CuTl-1223 superconducting matrix. The presence of different elements in these $(MnFe_2O_4)_x/CuTl\text{-}1223$; x = 0 and x = 1.0 wt.% composites was determined by energy dispersive X-rays (EDX) spectroscopy as shown in Figure 4. The wt.% of different elements present in $(MnFe_2O_4)_x/CuTl\text{-}1223$; x = 0 and x = 1.0 wt.% composites are given in Table 2.
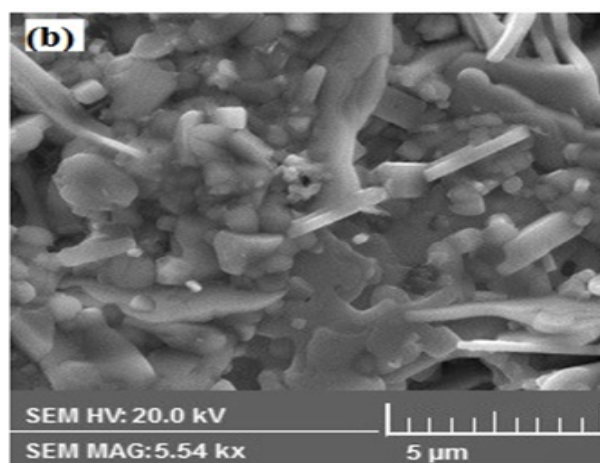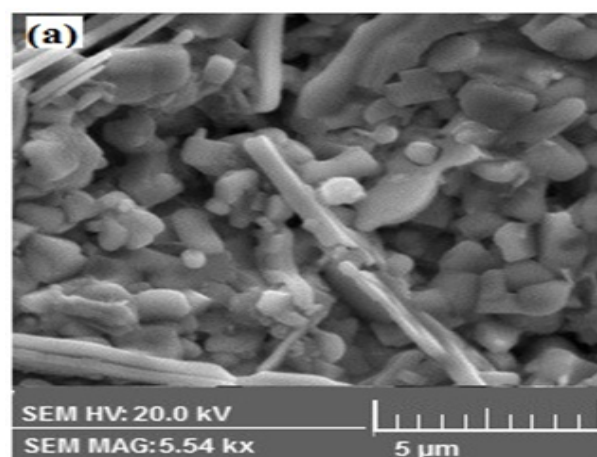

Figure 3. SEM images of $(MnFe_2O_4)_x/CuTl\text{-}1223$ composites with (a) x = 0, (b) x = 1.0 wt. %.

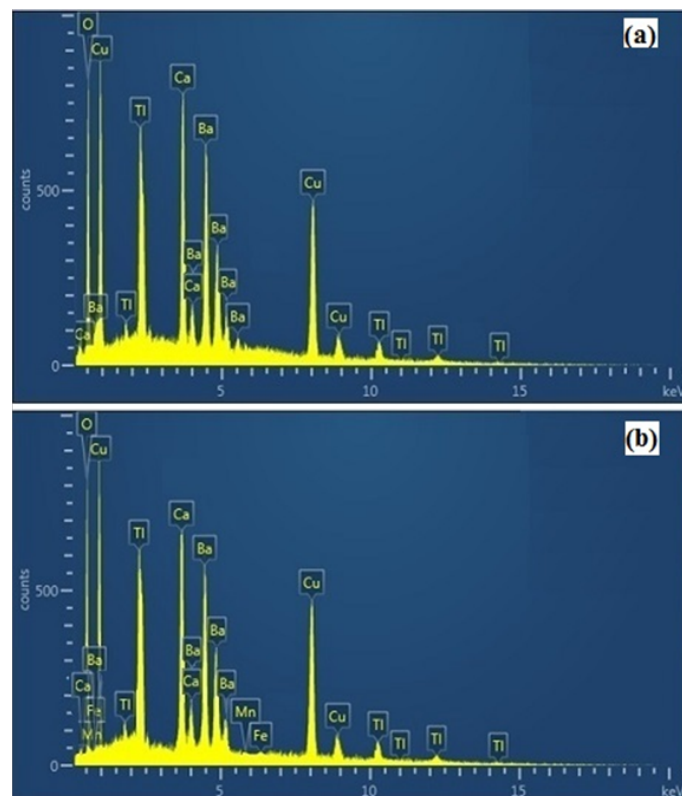**Figure 4**. EDX spectra of $(MnFe_2O_4)_x/CuTl\text{-}1223$ composites with (a) x = 0, (b) x = 1.0 wt. %.

Table 2. % of different elements present in $(MnFe_2O_4)_x/CuTl-1223$; x = 0, 1.0 wt.% nanoparticles-superconductor composites.

Elements	wt.% of elements in samples with x = 0	wt.% of elements in samples with x = 1.0 Wt.%
O	16.5	18.9
Ca	9.20	8.9
Cu	27.7	23.8
Ba	28.6	28.8
Tl	18.0	18.0
Fe	---	1.0
Mn	---	0.5
Total %	100	100

The trace amount of impurities and different functional groups can be identified with the help of FTIR spectroscopy. Different vibrational oxygen modes in unit cell of cuprates can also be investigated by FTIR absorption spectroscopy. Different oxygen vibrational phonon modes in our samples has been studied by FTIR absorption spectroscopy as we know optimum oxygen content are very useful for superconductivity in HTSCs. FTIR absorption spectra of $(MnFe_2O_4)_x/CuTl-1223$ composites in the range from 400 to 700 cm^{-1} are shown in Figure.5. The absorption modes appearing in the range from 400 to 540 cm^{-1} are associated with apical oxygen atoms and 541 - 600 cm^{-1} represents the modes of CuO_2 planer oxygen atoms[22]. The modes in the range from 600 to 700 cm^{-1} are associated with O_δ oxygen atoms in the charge reservoir layers. Apical oxygen modes of type Tl-O_A-Cu(2) and Cu(1)-O_A-Cu(2) and planner oxygen modes of type Cu(2)-Op-Cu(2) can be observed around 420 cm^{-1}, 459 cm^{-1} and 543 cm^{-1}, respectively for un-added pure CuTl-1223 sample. All absorption bands almost remained unchanged after the addition of $MnFe_2O_4$ nanoparticles. By comparing the FTIR absorption spectra of pure and nanoparticles added samples, we found that the stoichiometry and structure of host CuTl-1223 matrix remained un-disturbed after the inclusion of these $MnFe_2O_4$ nanoparticles. Therefore, FTIR absorption spectroscopy also indicated the occupancy of these nanoparticles at inter-granular sites of host CuTl-1223 matrix.
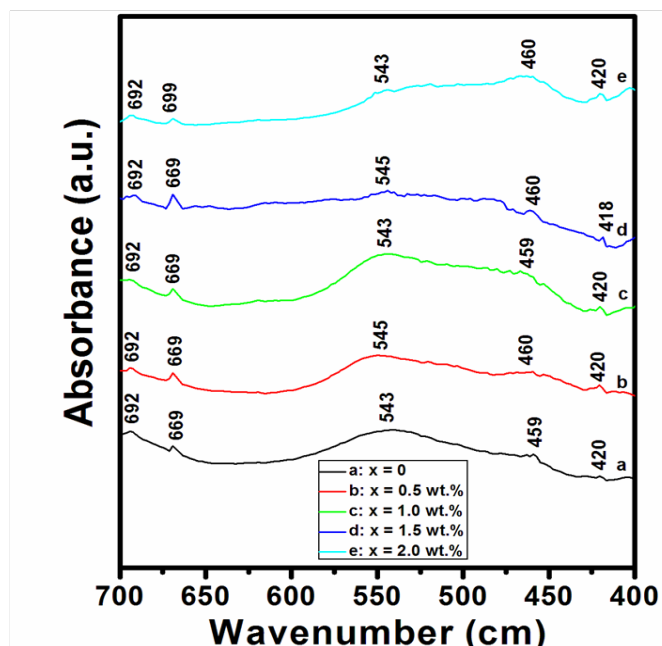

Figure 5. FTIR absorption spectra of $(MnFe_2O_4)_x/CuTl-1223$ composites with (a) x = 0, (b) x = 0.5 wt.%, (c) x = 1.0 wt.%, (d) x = 1.5 Wt.% and (e) x = 2.0 wt. %.

The resistivity versus temperature measurements of $(MnFe_2O_4)_x/CuTl-1223$; (x = 0, 0.5, 1.5 and 2.0 wt.%) nanoparticles-superconducting composites are shown in Figure 6. The variation of T_c^{onset} (K) with respect to various concentrations of $MnFe_2O_4$ nanoparticles in CuTl-1223 superconducting matrix is shown in the inset of Figure 6. Normally T_c^{onset} (K) depends upon electronic properties of given material while T_c (0) depends upon micro-structural characteristics of material and carrier's density in CuO_2 planes[23-27]. After the addition of $MnFe_2O_4$ nanoparticles, the value of T_c^{onset} (K) was decreased, which showed the reduction in superconducting volume fraction and cooper pairs formation across transition from normal state to superconducting state. The reduction in cooper pairs formation is most probably due to enhanced scattering cross-section caused by the magnetic nature of these particles. Therefore, these nanoparticles act as affective scattering centers at grain-boundaries due to which overall all superconductivity was suppressed.
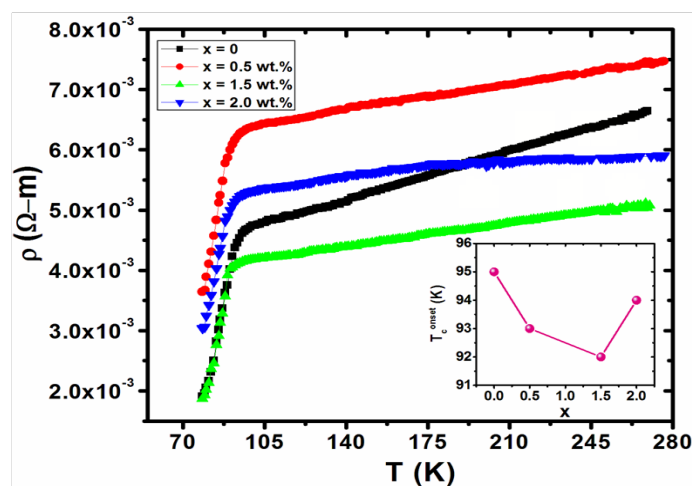

Figure 6. Resistivity versus temperature measurements of $(MnFe_2O_4)_x/CuTl-1223$ composites with x = 0, 0.5, 1.5 and 2.0 wt. % and in the inset is shown the variation in T_c^{onset} (K) with nanoparticles content (x).

Conclusion

The effects of magnetic $MnFe_2O_4$ nanoparticles addition on micro-structural, morphological and transport characteristics of CuTl-1223 phase were studied and compared. The crystal structure and stoichiometry of CuTl-1223 phase were not influenced by the addition of these nanoparticles at grain-boundaries. The suppression of superconductivity was observed with inclusion these nanoparticles. Superconducting volume fraction and cooper pairs density was suppressed due to enhanced scattering cross-section across these magnetic nanoparticles at grain-boundaries. Most challenging problem in these superconducting composites is to make uniform and homogeneous distribution of $MnFe_2O_4$ nanoparticles or any other nanostructures at grain-boundaries of host CuTl-1223 superconductor. Therefore, somehow non-monotonic behavior in variation of normal state resistivity and other superconducting parameters of $(MnFe_2O_4)_x/CuTl-1223$ composites was observed, which was associated with inhomogeneous distribution of $MnFe_2O_4$ nanoparticles at the grain-boundaries of bulk CuTl-1223 superconducting phase.

References

1. Ihara, H., Tanaka, K., Tanaka, Y., et al. Mechanism of Tc enhancement in $Cu_{1-x}Tl_x$-1234 and-1223 system with Tc >130 K. (2000) Physica C 341-348(1): S487-S488.
CrossRef | Others

2. Acharya, S., Biswal, A.K., Ray, J., et al. Study of $Bi_2Sr_2CaCu_2O_8$/$BiFeO_3$ nano-composite for electrical transport applications. (2012) J Appl Phys 112(5).
CrossRef | Others

3. Pu, M.H., Song, W.H., Zhao, B., et al. Enhanced flux pinning in (Bi, Pb)-2223/Ag tapes by slight Pr substitution. (2001) Supercond Sci Technol 14(6).
CrossRef | Others

4. Miura, M., Kato, T., Yoshizumi, M., et al. Enhancement of flux pinning in $Y_{1-x}Sm_xBa_{1.5}Cu_3O_y$ coated conductors with nanoparticles. (2008) Appl Phys Express 1(5).
CrossRef | Others

5. Engel, S., Thersleff, T., Huhne, R., et al. Enhanced flux pinning in $YBa_2Cu_3O_7$ layers by the formation of nano-sized $BaHfO_3$ precipitates using the chemical deposition method. (2007) Appl Phys Lett 90(10).
CrossRef | Others

6. Puig, T., Gutierrez, J., Pomar, A., et al. Vortex pinning in chemical solution nanostructured YBCO films. (2008) Supercond Sci Technol 21(3).
CrossRef | Others

7. Strickland, N.M., Long, N.J., Talantsev, E.F., et al. Enhanced flux pinning by $BaZrO_3$ nanoparticles in metal-organic deposited YBCO second-generation HTS wire. (2008) Physica C 468(3): S183-S189.
CrossRef | Others

8. Miura, M., Yoshizumi, M., Izumi, T., et al. Formation mechanism of $BaZrO_3$ nanoparticles in $Y_{1-x}SmxBa_2Cu_3Oy$-coated conductors derived from trifluoroacetate metal-organic deposition. (2009) Supercond Sci Technol 23(1).
CrossRef | Others

9. Abou-Aly, A.I., Gawad, M.M.H.A., Awad, R., et al. Improving the physical properties of (Bi, Pb)-2223 phase by SnO_2 nano-particles addition. (2011) J Supercond Nov Magn 24: S2077.
CrossRef | Others

10. Jia, Z.Y., Tang, H., Yang, Z.Q., et al. Effects of nano-ZrO_2 particles on the superconductivity of Pb-doped BSCCO. (2000) Physica C 337(1-4): S130-S132.
CrossRef | Others

11. Annabi, M., Mchirgui, A., Azzouz, F.B., et al. Addition of nanometer Al_2O_3 during the final processing of (Bi, Pb)-2223 superconductors. (2004) Physica C 405(1): S25-S33.
CrossRef | Others

12. Christova, K., Manov, A., Nyhus, J., et al. $Bi_2Sr_2CaCu_2O_x$ bulk superconductor with MgO particles embedded. (2002) J Alloys Compd 340(1-2): S1-S5.
CrossRef | Others

13. Ghattas, A., Azzouz, F.B., Annabi, M., et al. Pinning mechanism in (Bi, Pb)-2223 polycrystalline samples prepared with Al_2O_3 nano-particles. (2008) J Phys: Conf Ser 97(1).
CrossRef | Others

14. Mohammed, N.H., Abou-Aly, A.I., Awad, R., et al. Mechanical and electrical properties of $(Cu_{0.5}Tl_{0.5})$-1223 phase added with nano-Fe_2O_3. (2013) J Low Temp Phys 172(3): S234-S255.
CrossRef | Others

15. Li, A.H., Ionescu, M., Liu, H.K., et al. Microstructures and enhancement of critical current density in $YBa_2Cu_3O_7$ thin films grown by pulsed laser deposition on various single crystal substrates modified by Ag nano-dots. (2005) IEEE Trans Appl Supercond 15(2).
CrossRef | Others

16. Bartunek, V., Smrckova, O. Preparation of the silver-superconductor composite by deposition of the silver nanoparticles in the bismuth cuprate superconductor. (2011) J Supercond Nov Magn 24(4): S1241-S1244.
CrossRef | Others

17. Abdeen, W., Mohammed, N.H., Awad, R., et al. Influence of nano-Ag addition on the mechanical properties of $(Cu_{0.5}Tl_{0.5})$-1223 superconducting phase. (2013) J Supercond Nov Magn 26(11): S3235-S3245.
CrossRef | Others

18. Awad, R., Abou Aly, A.I., Mohammed, N.H., et al. Investigation on superconducting properties of $GdBa_2Cu_3O_{7-\delta}$ added with nanosized ZnFe2O4. (2014) J Alloys Compd 610: S614-S622.
CrossRef | Others

19. Slimani, Y., Hannachi, E., Hamrita, A., et al. Comparative study of nano-sized particles $CoFe_2O_4$ effects on superconducting properties of Y-123 and Y-358. (2014) Physica B 450: S7-S15.
CrossRef | Others

20. Jabbar, A., Qasim, I., Khan, S.A., et al. Highly coercive cobalt ferrite nanoparticles-CuTl-1223 superconductor composites. (2015) J Magn Magn Mater 377: S6-S11.
CrossRef | Others

21. Ihara, H., Tokiwa, K., Iyo, A., et al. New high-Tc superconductor families of $Ag_{1-x}Cu_xBa_2Ca_{n-1}Cu_nO_{2n+3-y}$ and $CuBa_2Ca_{n-1}Cu_nO_{2n+4-y}$ with Tc > 116 K. (1994) Physica C 235-240(2): S981-S982.
CrossRef | Others

22. Firdous, T., Khan, N.A. Sn doped $(Cu_{0.5}Tl0.5)$ $Ba_2Ca_2Cu_{3-y}S_{ny}O_{10-\delta}$ superconductors: Effect on the diamagnetism and phonon modes. (2009) J Appl Phys 106(8).
CrossRef | Others

23. Kong, W., Abd-Shukor, R. Enhanced electrical transport properties of nano $NiFe_2O_4$-added $(Bi_{1.6}Pb_{0.4})Sr_2Ca_2Cu_3O_{10}$ superconductor. (2010) J Supercond Novel Magn 23: S257.
CrossRef | Others

24. Novosel, N., Pajic, D., Skoko, Z., et al. The influence of $CuFe_2O_4$ Nanoparticles on Superconductivity of MgB_2. (2012) Phys Procedia 36: S1498-S1503.
CrossRef | Others

25. Ke, C., Cheng, C.H., Yang, Y., et al. Flux pinning behaviour of MgB_2 doped with Fe and Fe_2O_3 nanowires. (2012) Phys Procedia 27: S40-S43.
CrossRef | Others

26. Novosel, N., Babic, E. Influence of magnetic nanoparticles on superconductivity of MgB_2. (2013) Physica C 493: S119-S124.
CrossRef | Others

27. Tarascon, J.M., Barboux, P., Miceli, P.F., et al. Structural and physical properties of the metal (M) substituted $YBa_2Cu_{3-x}M_xO_{7-y}$ perovskite. (1988) Phys Rev B Condens Matter 37(13): S7458-S7469.
Pubmed | CrossRef | Others